Journal of Nuclear Materials 604 (2025) 155471

Contents lists available at ScienceDirect

Journal of Nuclear Materials

journal homepage: www.elsevier.com/locate/jnucmat

DFT simulations of the self-healing behavior of a W⟨110⟩/W⟨112⟩ grain boundary in the presence of coexisting point defects

J. Suárez-Recio [a,b,c,*], D. Fernández-Pello [c], M.A. Cerdeira [c], C. González [d,e], R. Gonzalez-Arrabal [a,b], R. Iglesias [c,f]

[a] Instituto de Fusión Nuclear "Guillermo Velarde", Universidad Politécnica de Madrid, Madrid, E-28006, Spain
[b] Departamento de Ingeniería Energética, Universidad Politécnica de Madrid, Madrid, E-28006, Spain
[c] Departamento de Física, Universidad de Oviedo, Oviedo, E-33007, Spain
[d] Departamento de Física de Materiales, Universidad Complutense de Madrid, Madrid, E-28040, Spain
[e] Instituto de Magnetismo Aplicado UCM-ADIF, Las Rozas, E-28006, Spain
[f] Centro Universitario ASturias RAw Materials Institute (ASRAM), Universidad de Oviedo, Mieres, E-33600, Spain

ARTICLE INFO

Keywords:
Metallic interfaces
Grain boundaries
Defects
Helium
Hydrogen
Ab-initio simulations
Density functional theory
Self-healing

ABSTRACT

Light impurity atoms (LIAs), such as hydrogen and helium, tend to aggregate at pre-existing intrinsic point defects. This aggregation leads to detrimental effects, particularly in environments such as those foreseen in nuclear fusion reactors. There, such impurities would be ubiquitous, resulting in unacceptable material behavior that would unqualify the material as a Plasma Facing Material (PFM). One option to delay the degradation in performance is the use of nanostructured tungsten (NW), showing a large density of grain boundaries (GBs). Although we have already addressed the behavior of a single LIA in a GB, in this work we present the combined synergistic effects of the simultaneous presence of multiple LIAs, vacancies and Self-Interstitial Atoms (SIA) at semicoherent W/W interfaces using ab initio methods. Our results reveal a complex and interesting process in the competition between LIAs and SIAs. When the number of SIAs is low, He appears to hinder their recombination with vacancies, therefore casting doubts on the self-healing provided by NW. However, in the presence of larger numbers of SIAs, their mutual repulsion leads to the opposite behavior. Thus, a thorough thermodynamic assessment in which the evolution of the system may be tracked emerges as the crucial subsequent step in these investigations.

1. Introduction

Nuclear fusion has become one of the most promising concepts for a future large-scale energy supply, due to the high amount of energy released during the fusion process. It fits perfectly into the 2030 agenda, since it will provide accessible (fuel elements Li and D are widely distributed), sustainable and CO_2-free energy.

For more than half a century, researchers around the world have attempted to achieve ignition as a proof-of-concept for various fusion approaches. Fortunately, on August 2021, this milestone was achieved for the first time in an experiment carried out at the National Ignition Facility (NIF) [1–3]. This experiment represented a great leap forward, as it demonstrated that the ignition threshold is real, largely consistent with theoretical expectations, and that plasma ignition can be achieved in an experimental reactor, i.e., at the laboratory scale. However, in this first experiment no energy gain (Q) was obtained. Subsequently, in some experiments performed in 2022 and throughout 2023, at the same facility, the feasibility of energy gain was also demonstrated. These breakthroughs have motivated a significant increase in public and private funding for the development of projects aimed at the conceptualization of commercial power plants.

Despite the achievements, there is still a number of challenges that need to be addressed prior to up-scaling to a commercial facility. One of them is the development of plasma facing materials (PFMs) able to withstand the combined effects of large thermal loads and aggressive irradiation environments which take place in these reactors.

Because of its properties, commercial, coarse grained W (CGW) has been suggested to be the best candidate for a PFM in nuclear fusion reactors [4]. However, it has some drawbacks [5–7], among which its high capacity to retain light species, which are insoluble in metals, but very mobile, can be trapped by vacancies and any other defect present in the material. Moreover, in the absence of traps, when the number of He

* Corresponding author.
E-mail address: j.srecio@upm.es (J. Suárez-Recio).

https://doi.org/10.1016/j.jnucmat.2024.155471
Received 9 June 2024; Received in revised form 26 September 2024; Accepted 18 October 2024
Available online 23 October 2024

atoms is large enough they have also been observed to form clusters that produce a large strain in the matrix. To release this strain, one or more interstitials are emitted, creating vacancies that can trap the He clusters they have created. This phenomenon is called self-trapping. When vacancies are associated with the He clusters, the mechanism is activated and is called trap mutation. However, according to previous publications, for self-trapping and/or trap mutation to occur, the number of He atoms in the absence of an initial vacancy must be ≥ 5 and even larger (≥ 13) if a previous vacancy exists [8]. This accumulation of LIAs in W strongly limits its lifetime [9–24]. Indeed, even if the incident neutrons are obviously detrimental to the material, leading to swelling, cracking, and a decrease in thermal conductivity in the long term (years), [25–29] the lifetime of PFMs will be dictated by the deleterious effects of impinging ions, in particular of light ions. For instance, the estimated lifetime for CGW as a PFM in the HiPER-DEMO reactor based on synergistic effects, thermal loads accompanied by He irradiation, would be of only some seconds [30].

Consequently, some alternative materials such as nanostructured W (NW) in which the grain size has been reduced down to the nanometric scale, notably increasing the density of grain boundaries (GBs) [31–40] and W-based engineered surfaces such as W nanoneedles [41–49], with a large surface area, have been suggested as alternative materials for PFM applications even when the thermal stability of NW under predicted reactor working conditions remains an open question that requires further investigation [50].

These substitute materials have shown, under certain circumstances, a higher radiation resistance than CGW. However, because of the lack of experimental facilities able to mimic the synergistic effects taking place in nuclear fusion reactors (i.e., atomistic damage produced by the simultaneous arrival of neutrons, He, and, H-isotopes concomitant to large thermal loads), in particular in those operating in the inertial confinement approach (ICF) [30], and because of the difficult and time-consuming simulations, most of the studies have been devoted to analyze the simpler behavior of these alternative materials under pure He or H irradiation in the presence or not of thermal loads.

Focusing on NW, most of the previously reported data for samples irradiated with ions (He and H) impinging in the high energy range (hundreds of keV), at energies above the displacement damage threshold (E_d =90 eV) [51], in which Frenkel pairs (vacancies and self-interstitial atoms, SIAs) are created, were devoted to study the radiation effects in the low temperature regime, at which vacancies are immobile. These data, in agreement with the three-temperature model of Beyerlein et al. [52], show that GBs behave as defect sinks and that, at those temperatures, vacancies remain in the interior of the grain in the region where they were created [53]. At higher temperatures, such as those taking place in fusion reactors (e.g., 800 °C for the HiPER steady state and up to ~3400 °C for the HiPER-DEMO immediately after the arrival of ions [54]), the radiation response of these materials is predicted to be different, since at these temperatures vacancies are already mobile (~300 °C) [55,56]. Thus, they are expected to reach the GBs where the SIAs are located and recombine with them, a phenomenon known as self-healing process. So far, to the best of our knowledge, there is a little evidence of this in NW [36].

In an ICF reactor, not only SIAs are predicted to be present at the GB but also, He and H. Therefore, the obvious question to be asked is if having He and H at the GB would influence the self-healing behavior since both LIAs could either migrate to the GB and remain there or, on the contrary, escape using the GB as a pathway. It is important to mention that, regardless of the differences in energy and fluxes, this situation is going to be similar to that happening in the divertor of magnetic confinement fusion (MCF) reactors in which the energy of the impinging ions (keV) is also expected to be above the displacement damage threshold.

This question was addressed in a previous paper [37], in which the authors reported on ab initio simulation results focused on completing a thorough energetic, structural, charge and mobility analysis of the synergistic behavior of a SIA and up to two LIAs (one He and one H), showing that the introduction of a SIA into a GB preloaded with H and He, drives the He to be attracted to the SIA while H prefers to stay away from it. In other words, the presence of He could prevent the SIA from filling in the vacancy and thus hinder the self-healing process (SIA-vacancy recombination).

This article provides a logical extension of the aforementioned paper considering a larger number of atoms. To do so, we have increased the numbers of each defect type (SIA, He and H) on a W⟨110⟩/W⟨112⟩ GB containing a pre-existing vacancy to study the possible competition effects. Our Density Functional Theory (DFT) simulations have been carried out in a very systematic way by performing an energetic, structural, electronic and diffusivity analysis for different configurations in the presence of the most stable vacancy: (i) *n*He and *n*H, (ii) *n*SIAs and *n*H, (iii) *n*SIAs and *n*He, (iv) *n*SIAs, *n*H and *n*He, where *n* is between 1 and 3 and accounts for the number of atoms of each type.

2. Methodology

All calculations in this paper have been performed using the DFT framework [57] employing the plane-wave Vienna Ab initio Simulation Package (VASP) [58]. Projector augmented-wave (PAW) pseudopotentials (PP) [59] were used under the generalized gradient approximation (GGA), proposed in the Perdew-Burke-Ernzerhof (PBE) formalism [60]. The W PP included 6 electrons in the valence band (corresponding to the most usual configuration $5d^4 6s^2$). The H and He PPs were also characterised by their conventional $1s^1$ and $1s^2$ electronic configurations, respectively. Using the procedures described above, we have found the lattice parameter of W to be 3.172 Å, which is in good agreement with the experimental value of 3.165 Å [61]. The plane wave cutoff energy was set at 400 eV and relaxation was deemed to have been achieved when the Hellmann-Feynman forces on the ions were no greater than 0.03 eV $Å^{-1}$.

The construction of the W⟨110⟩/W⟨112⟩ interface has already been explained in great detail in previous articles [33,40]. Briefly, it consists of two 6-layer slabs along the Z-axis, i.e., 288 (168) atoms in W⟨110⟩ (W⟨112⟩). It is based on the coincidence lattice site (CSL) theory [62], that is a geometrical construction derived from the geometry of the lattice. In this theory, the rotation of the second lattice, i.e., top/bottom surface, is limited to those values that bring a (lattice) point into coincidence with another point in the first lattice. Specifically, we have rotated the (110) surface 55 degrees with respect to the (112) surface. However, due to the non-coherent nature of the interface, the W⟨112⟩ surface has been expanded by about 1% in the X-direction. Regarding the k-point mesh, due to the large dimensions of the system (31.09 Å ×10.98 Å ×31.72 Å), only the gamma point at the center of the Brillouin zone was used, as it was found to be sufficiently accurate [37]. We have fixed the last two layers at each side, to resemble bulk-like conditions. The rest of the atoms are allowed to relax until they fit the convergence criteria. In addition, we have included a free vacuum of 12 Å to eliminate the undesired residual interactions between adjacent layers when the cell is repeated in the Z-direction. A full optimization of atomic positions after introducing the defects is performed in two steps, to try to significantly reduce the probability of running into convergence problems. First, we relax the system via a damped Molecular Dynamics force-based optimization that implements a robust line search algorithm. Once this initial step is completed, the system is further relaxed by using the conjugate gradient algorithm with a scaling constant for the step widths of 0.5 Å.

With respect to the energetic analysis, we are focused mainly on formation energies, E_f, and interaction energies, E_i. The formation energy of a system $E_f(N_M, N_{SIA}, N_H, N_{He})$, containing N_M W atoms, N_{SIA} SIA and $N_{LIA} = N_H + H_{He}$ LIA atoms, where obviously N_H (N_{He}) stands for the number of H (He) atoms, can be easily estimated using the corresponding total energies taken from the DFT simulations. We can define it as follows:

$$E_f(N_M, N_{SIA}, N_H, N_{He}) = E(N_M, N_{SIA}, N_H, N_{He}) - N_{SIA}E^{ref}(M) - N_H E^{ref}(H) - N_{He}E^{ref}(He) - E(N_M, 0, 0, 0), \quad (1)$$

where the final energy obtained is expressed as $E(N_M, N_{SIA}, N_H, N_{He})$ and $E(N_M, 0, 0, 0)$ corresponds to the pristine configuration without defects. Here, $E^{ref}(M)$, $E^{ref}(He)$ and $E^{ref}(H)$ are the reference energies of the different species present in the system, i.e., the energy per metal atom and those of the two possible species of LIAs. The reference energy of a metallic atom is obtained from a perfect crystal, considered to be a 5×5×5 bcc supercell; $E^{ref}(He)$ and $E^{ref}(H)$ are, respectively, the energy of an isolated He atom and half the energy of an H_2 molecule when both objects are placed inside a large empty simulation box.

Additionally, one can define the interaction energy, E_i, between two configurations by subtracting from the energy of the system with the LIAs and SIAs $E(M, SIA, He, H)$ firstly the contribution of the impurity that is removed, say H (analogously for the He and SIA), $E(H)$, calculated inside the large empty supercell used for the total energy simulations, and secondly the contribution of the remaining metallic atoms and the He and SIA atoms $E(M, SIA, He)$. The latter is calculated by removing the H and constraining the metallic atoms to be fixed at the positions that are found from the relaxation of the structure when the H atom was still present. The same reasoning is valid for the He and SIA cases. Therefore, the equation that represents the interaction between H and the metal can be expressed as follows:

$$E_i(M, SIA, He, H) = E(M, SIA, He, H) - E(H) - E(M, SIA, He). \quad (2)$$

By using this definition, a positive value indicates that removing a LIA results in a lower energy configuration, while a negative value implies the opposite. This approach provides insight into the potential energy change attributed solely to the presence of the impurity within a fixed lattice configuration, helping to isolate the energetic contribution of the impurity alone. The interaction energy highlights how the defect affects the local environment before any relaxation occurs and is believed to be valuable for comparative studies involving different defects or impurities under the same conditions [36].

Next, the concepts of Voronoi and Bader volumes are introduced. The Voronoi volume [63] refers to the space around each atom that is closer to it than to any other atom, providing insight into the geometric arrangement of atoms within a structure. On the other hand, the Bader volume [64] is associated with the electronic density around each atom, offering information about charge distribution and electron localization. It is important to note that, while both volumes offer valuable insights into the spatial distribution within a system, they serve different purposes and are not directly comparable.

Finally, the mobility of defects in selected cases to evaluate the effect of the simultaneous presence of multiple defects has been analyzed. The aim has been to calculate the energy barriers required to evolve the system between two stable, relevant configurations, as found in the previous steps. The Nudged Elastic Band (NEB) method as implemented in VASP [65] to find the most favorable trajectory showing the lowest migration barrier has been used. This method helps to minimize the energetic cost for a displacement from one initial to a final equilibrium configuration, following the prescriptions of Transition State Theory (TST) [66]. The energy barrier has been calculated by subtracting the total energy at the initial equilibrium configuration from the one at the saddle-point. For each migration, a total of 9 images (#1-#9) were initially generated, with the first and last corresponding to equilibrium configurations. The initial coordinates of all atoms in the intermediate images #2 to #8 were set to values linearly interpolated between images #1 and #9. In our NEB calculations, each #M image was linked to the #(M-1) and #(M+1) images with an inter-image string constant of 5.0 eV/Å^2 and a maximum allowed translation step of 0.25 Å. The multi-image minimization procedure was processed using the force-based Fast Inertial Relaxation Engine (FIRE) method [67] until a predetermined tolerance value for the force of 0.1 eV/Å was reached.

In all calculations shown in the following, He self-trapping and trap mutation have been left out of account because, as mentioned in the introduction, the reported number of He atoms for these phenomena to occur is, in any case, larger than the one we consider [8]. Zero point energy (ZPE) contributions have also been disregarded, because even if they may have an effect on solution energies [68], their influence on formation energies has a minor effect [69].

3. Results

In this section we present the results of our DFT calculations on the behavior of NW under simultaneous He and H irradiation at energies above the displacement damage threshold. Fig. 1 shows the most stable vacancy at the GB (green sphere), viewed from the front (or above) in a) and from both the two sides in b) and c). Note that the vacancy is located at the (112) surface, as determined in a previous article [33]. All subsequent calculations are performed with this vacancy present.

To determine which LIA species occupies the vacancy first, we placed defects (up to 3 of each) along the grooves adjacent to the vacancy, marked by red arrow lines and dashed circles in Fig. 1 a) and b), respectively. To ensure that we identified the most stable configuration, for each set of defects we systematically generated three different initial configurations based on plausible atomic arrangements around the GB and the vacancy. Each configuration was then relaxed to allow the system to reach a local energy minimum. We then compared the energy of these relaxed structures to identify the most stable (i.e., lowest energy) configuration. Figs. 2, 4, 6, and 10 correspond to the red insets in Fig. 1 b) and c), and show the various relaxed interface configurations. Each arrangement is discussed below.

3.1. He and H aggregates in the presence of the most stable vacancy

First, we describe the coexistence of He, H and the most stable vacancy to find out which LIA tends to preferentially occupy the latter, depending on the number of defects of each type. Our results, depicted in Fig. 2, show that for all the studied configurations, He atoms occupy the pre-existing vacancy, while H atoms remain inside the groove. These results agree with previously reported data for W bulk [70,71], which show that the binding energy to a vacancy is larger for He (∼4 eV) than for H (∼1.4 eV). Moreover, they also evidence that the migration barrier to reach a vacancy is lower for He (0.06 eV) than for H (0.14 eV). This may be due to the fact that, as a noble gas, He does not interact (or at least not strongly) with other atoms in the lattice, although it is more comfortable in regions of lower charge density, dark blue areas in Fig. 1 d)-e), where repulsive interactions between He and the metal atoms are minimal [40,72]. As may be envisaged from Fig. 1 d), He atoms are expected to migrate from the bulk in the plane perpendicular to the interface grooves and subsequently aggregate inside the low charge density regions. In addition, Fig. 1 d) shows that the charge density along the grooves is not uniform. This lack of uniformity is mainly related to the irregularities of the interface geometry. Moreover, as expected, the lowest charge density values are found to be around the most stable vacancy. These values are lower than those of the interface and much lower than those of the inner layers. Specifically, for configurations with 3 He atoms (Fig. 2 g)-i)), one of those He atoms tends to occupy the vacancy, while the other two draw up and end sitting at an intermediate position between the vacancy and the groove. It is important to clarify that our results do not imply that a vacancy can only accommodate one He atom. In the presence of the GB, He atoms initially located within the GB feel a slight attraction to the vacancy, even if it is already occupied by another He atom. However, instead of aggregating inside the vacancy, they tend to settle around it, finding the occupation of the surrounding low-charge regions more energetically fa-

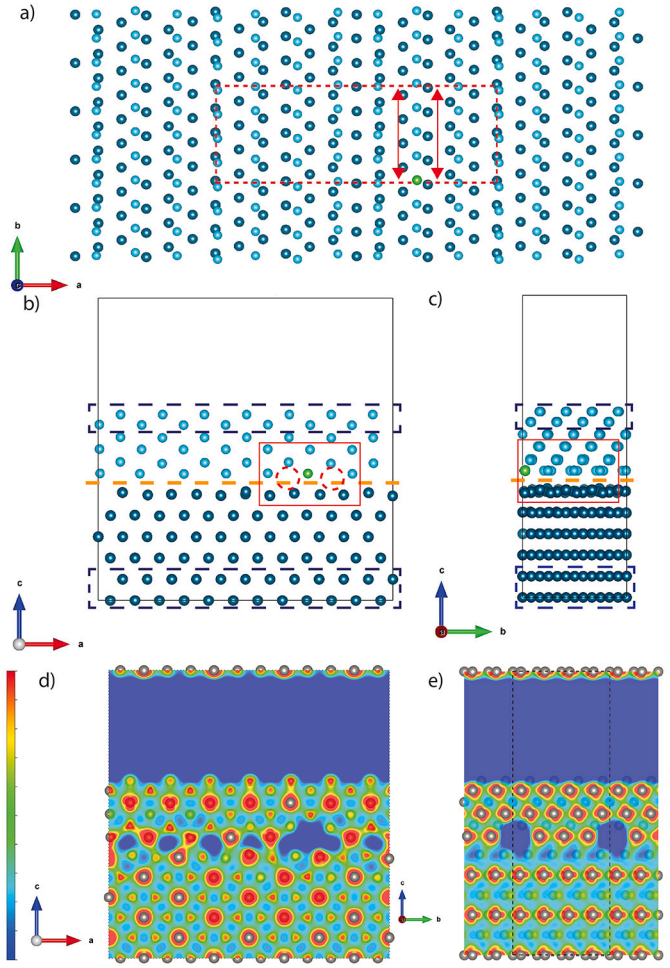

Fig. 1. (color on-line) a) Frontal view of the W⟨110⟩/W⟨112⟩ GB, where the light (dark) blue spheres represent the W atoms in the (112)[(110)] surface, while the green sphere corresponds to the most stable vacancy position [33]. The dashed red line denotes the edges of the simulation box, while red arrows illustrate the grooves where defects are stored. b) and c) GB as viewed from the Y-axis and X-axis, respectively, that is, from the sides parallel to the interface (indicated with an orange dashed line). The atoms inside blue dashed boxes were fixed to simulate bulk-like conditions. d) and e) Charge density distribution of the interface viewed from the Y-axis and X-axis, respectively, in the presence of the most stable vacancy.

vorable. This arrangement allows them to minimize their energy while still being influenced by the presence of the vacancy.

Conversely, the H atoms seem to ignore the deformation of the electronic environment due to the vacancy and try to bind to one of the nearest metal atoms in order to minimize the deformation of the system. The distance between each H atom and its nearest W neighbor falls within the range between 1.87 and 1.98 Å for all cases. Since this distance is larger than the bonding H-W in a W hydride, these results seem to indicate that the presence of H atoms does not lead to the formation of a W hydride. This is probably due to a combination of factors, including the positive formation energy of a W-H compound, the presence of other defects that compete for binding sites, and the differences in electronegativity and proton repulsion between W and H. For cases involving two and three H atoms, the situation is very similar to the previous one, namely, H atoms remain at the interface but do not align along the groove. Notably, in completing relaxation, all defects exhibit a slight approach toward the upper surface, i.e., the W⟨112⟩ surface.

To further investigate whether H atoms did not occupy the vacancy because the He atoms had already occupied that position, or whether H atoms inherently have no preference for the vacancy, we performed additional calculations in which only H atoms were introduced. The results confirmed that even in the absence of He, H atoms did not occupy the vacancy even though they do exhibit a preference for vacancies [33]. When H is initially located at the GB, it does not easily migrate to the vacancy due to the favorable local environment provided by the GB, which leads to a significant energy barrier to move into the vacancy (0.14 eV). This observation reinforces the idea that He, rather than H, is the primary competitor with SIAs for the vacancy site.

Table 1
Formation (E_f) and interaction energies (E_i) in eV for different LIA combinations at the GB.

Cluster (+ vac)	E_f (eV)	E_i He/H (eV)
He+H	3.47	1.47/−0.07
He+2H	3.13	1.56/−0.44
He+3H	3.21	1.57/0.02
2He+H	5.47	1.92/−0.32
2He+2H	5.46	1.55/−0.45
2He+3H	5.52	1.56/0.00
3He+H	7.86	1.95/−0.42
3He+2H	7.76	1.96/−0.45
3He+3H	7.93	2.17/0.01

Regarding the energetic analysis, Fig. 3 shows a histogram plot of the formation energies as a function of the number of He and H atoms. In addition, the numerical values of the formation energies are given in the second column of Table 1. Here we observe how E_f depends on the number of He, while the presence of H atoms does not seem to have any discernible effect. Examining the values in Table 1, it can be observed that for a given number of He atoms, the E_f is lower when 2 H atoms are introduced instead of 1 H. Specifically, the difference in E_f between 1 H and 2 H is 0.34 eV for 1 He, 0.01 eV for 2 He, and 0.10 eV for 3 He. This indicates that adding a second H atom reduces the formation energy, which may be surprising. One possible explanation for this behavior would be the formation of H molecules. The distances between H atoms in the different configurations have been consequently determined. When considering cases with two H, we observed that they are 2.17 Å, 2.10 Å, and 2.09 Å for, again, the configurations with 1, 2, and 3 He, respectively. These distances notably exceed the H-H bond length estimated from experimental data, which is approximately 0.74 Å, meaning that the H atoms are not forming H_2 molecules or strong chemical bonds with each other. This is further reinforced when considering configurations containing three H atoms. In this case, the distances between these H atoms vary within the range between 2.11 Å and 2.67 Å, again too large to form bonds. This is not surprising, as previous works report that H_2 molecules dissociate in different W environments such as bulk or surface [73–75].

The last column of Table 1 displays the interaction energies, providing a more in-depth analysis of our energetic findings. These data strengthen our earlier observations. The removal of a He atom leads to a more energetically favorable configuration due to its repulsive interaction with the surrounding metallic matrix. This change in energy is significantly larger compared to the removal of a H atom, which typically results in a much smaller energy change, given that the interaction between H and the matrix is generally only weakly attractive or neutral. Moreover, the incorporation of a third H atom consistently results in a nearly negligible interaction energy.

In order to perform a more comprehensive and complete assessment, we will proceed to examine the SIA+H case to analyze the extent to which H atoms can influence the recombination process.

3.2. SIA and H aggregates in the presence of the most stable vacancy

Now we turn our attention to the behavior of the SIA in the presence of H atoms, following a similar analysis as in the preceding subsection. Fig. 4 contains the 9 atomic models of the relaxed configurations. Again,

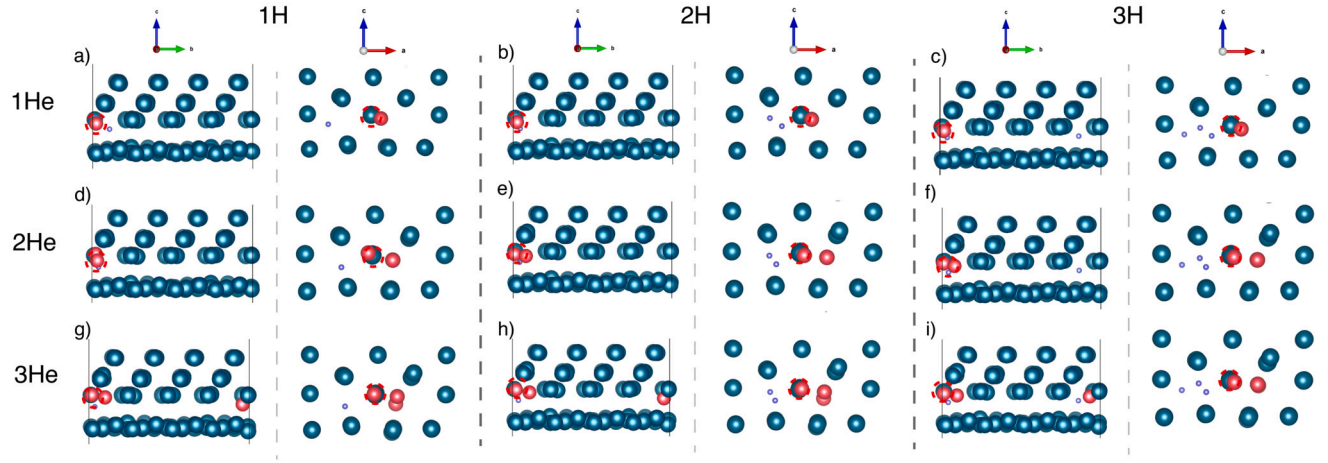

Fig. 2. (color on-line) YZ-plane (left column) and XZ-plane (right column) view of the 9 different relaxed He-H configurations. The three upper layers belong to the W⟨112⟩ surface, while the lower one belongs to the W⟨110⟩ surface. Purple and red spheres correspond, respectively, to H and He. The red dashed circles indicate the position of the vacancy.

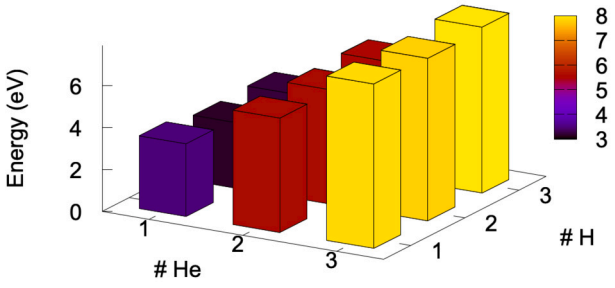

Fig. 3. Formation energies in eV as a function of the number of He and H.

in none of the cases do the H recombine with the vacancy; quite the contrary, they prefer to stay at the interface. On the other hand, the behavior of the SIAs depends on their number. When only one SIA is present, it seems to be more energetically stable for it to remain at the interface, regardless of the number of H atoms. From a purely geometrical viewpoint, the Voronoi volume occupied by the SIA, namely, 17.5 Å^3, may be compared to the available volume for the atoms of the inner layers close to the interface, which is about 15.5 Å^3. These numbers may be contrasted with the available volume provided by the vacancy, namely, 16.3 Å^3, i.e., an 8% smaller and a 5% larger, respectively, than the aforementioned values. Therefore, it seems quite reasonable for the SIA to remain in the GB. A similar phenomenon is observed when two SIAs are simultaneously present, i.e., they prefer to lie in a row at a consistent distance of 2.70 Å along the groove, rather than occupying the vacancy. In this case, the available volume for each of the SIAs is 15.2 Å^3 and 15.8 Å^3, respectively. These volumes are very similar to those in the bulk, meaning that the accommodation of the SIAs in these positions hardly deforms the system. However, when the 3 SIAs are present, the relaxation process leads to the recombination of the central one with the vacancy, while the remaining two interstitials end up placed along the groove in the same way as for the previous case with just two SIAs. The following subsection will provide a tentative explanation for this particular arrangement.

Fig. 5 illustrates the E_f as a function of the number of SIAs and H atoms. Similarly to the preceding subsection, it is observed that, when introducing a second H, the E_f decreases. If we calculate the distances between the H atoms, as previously done, we find that for cases with 2 H, these distances are approximately 2.25 Å, 2.17 Å, and 2.21 Å, depending on the number of SIAs. These values are slightly larger than the distances observed in the He+H configurations, indicating that the SIA-H interaction is even lower than the He-H one. When examining the distances for 3 H atoms, we observe that they are separated by values ranging

Table 2
Formation (E_f) and interaction energies (E_i) in eV for different SIA-H combinations at the GB.

Cluster (+vac)	E_f (eV)	E_i H/SIA (eV)
SIA+H	3.73	-0.03/-0.51
SIA+2H	3.42	-0.36/-0.41
SIA+3H	3.50	-0.34/-0.41
2SIA+H	4.97	0.14/-1.09
2SIA+2H	4.40	-0.39/-1.10
2SIA+3H	4.49	0.01/-0.66
3SIA+H	4.32	0.03/-2.05
3SIA+2H	4.27	-0.01/-0.43
3SIA+3H	4.33	0.01/-0.33

from 2.17 Å to 2.80 Å. Interestingly, the dependence of E_f on the number of SIAs follows a logical pattern. When a second SIA is added, E_f increases by about 1 eV in all three cases (see Table 2), most possibly due to the intrinsic difficulty in accommodating an extra large-sized interstitial. However, these energies seem to decrease slightly when we introduce the third SIA. Although at a first glimpse this could even be regarded as surprising, after following the relaxation process that leads to SIA-vacancy recombination of the central SIA, whereby this "extra" SIA finds a stable accommodation in a low charge density site, the outcome obviously enhances the stability of the system. If we compare the highest formation energy of the previous subsection, Table 1, i.e., 7.93 eV for the 3 He+3 H case, with that in Table 2, namely, 4.97 eV for the 2 SIA+1 H combination, we see that the latter is significantly lower, proving that it is the He that distorts the system the most.

The interaction energies shown in the Table 2 provide further insight into this behavior. As explained in the Methodology section, a negative interaction energy indicates that removal of a LIA (or SIA) would destabilize the system. Most of the studied cases have negative interaction energies, confirming that removing either SIAs or H atoms would reduce the stability of the system. This suggests that, at least for the small number of defects considered, GB can accommodate both SIAs and H more effectively than He. This will be explored in more detail in the following subsection.

In order to evaluate the influence of H atoms on the behavior of SIAs, we have also computed the E_f for the studied configurations of 1, 2, and 3 SIAs without the presence of H atoms. These calculations reveal that, qualitatively, the absence of H does not affect the interaction of the SIAs with the vacancy, i.e., recombination with the vacancy only occurs when 3 SIAs are present, as observed in the configurations with H.

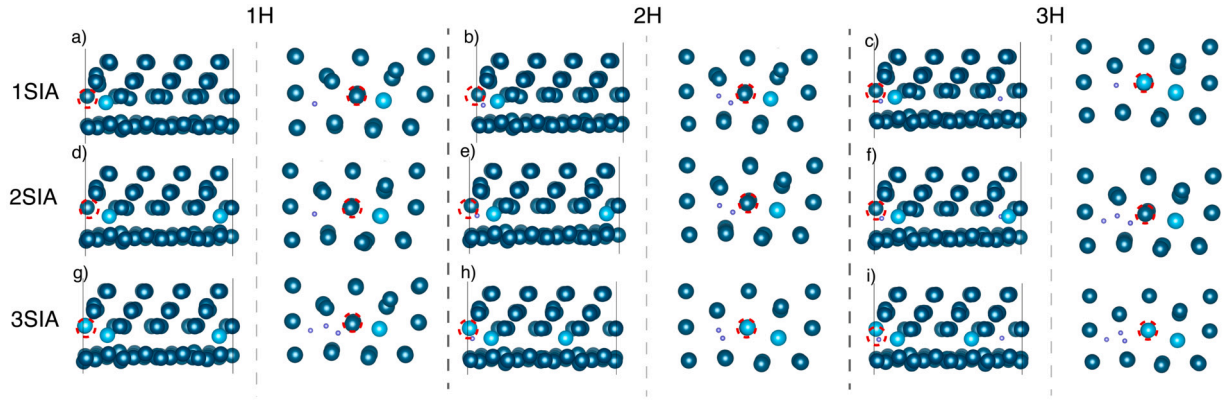

Fig. 4. (color on-line) YZ-plane (left column) and XZ-plane (right column) view of the 9 different relaxed SIA-H configurations. The three upper layers belong to the W⟨112⟩ surface, while the lower one belongs to the W⟨110⟩ surface. Purple and light blue spheres correspond, respectively, to H and SIA. The red dashed circles indicate the position of the vacancy.

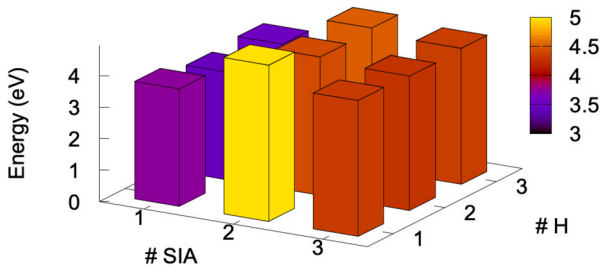

Fig. 5. Formation energies in eV as a function of the number of SIA and H.

From the analysis of these values, it can be seen that the E_f are slightly different in the absence of H atoms. For example, in the case of a single SIA, the energy is about 0.1 eV higher than when H is present. This difference could be due to the fact that the presence of H atoms in the regions close to the GB could stabilize the system by slightly reducing the energy, although, so far, we have no conclusive evidence for this. In the case of two and three SIAs, the E_f are both lower in the absence of H atoms, with differences of 0.74 eV and 1.09 eV, respectively. The largest difference, observed in the case of three SIAs, could be attributed to the fact that in the presence of H atoms, the SIA-vacancy recombination is influenced by the proximity of H atoms in adjacent layers, leading to a higher overall energy in the system. These results suggest that, while H atoms slightly modify the E_f of the SIA configurations, they do not qualitatively alter the recombination behavior of SIAs with vacancies at the GB, at least under the conditions explored in this study.

3.3. SIA and He aggregates in the presence of the most stable vacancy

In the following we examine the configurations with SIAs and He atoms. Our results show that in all configurations except those with 3 SIAs (as previously addressed in subsections 3.1 and 3.2), He tends to occupy the vacancy after relaxation, potentially hindering the desired self-healing process (see Fig. 6). As discussed in subsection 3.1, there are two reasons for this. First, as is well known [40], He tends to occupy regions of lower charge density, and second, it is less demanding for the SIA to accommodate the neighboring atoms, since there is already enough space available in the interface, than to migrate toward the vacancy.

The energetic analysis of the system indeed reveals interesting insights into its behavior. Fig. 7 and Table 3 summarize the formation and interaction energies in eV for all the different configurations. Fig. 7 shows a 3D histogram plot of the E_f as a function of the number of SIAs and He atoms. As expected, E_f increases substantially with the number of He atoms. Furthermore, whether it is the He or the SIA that occupies the vacancy does not seem to have any effect on E_f. All of this is

Table 3
Formation (E_f) and interaction (E_i) energies in eV for different SIA-He combinations at the GB.

Cluster (+vac)	E_f (eV)	E_i He/SIA (eV)
SIA+He	5.72	1.84/-0.23
SIA+2He	8.12	1.81/0.06
SIA+3He	10.66	1.53/-0.03
2SIA+He	6.47	1.85/-0.84
2SIA+2He	9.06	1.81/-0.83
2SIA+3He	9.73	1.79/-0.65
3SIA+He	6.56	2.96/-0.89
3SIA+2He	11.22	2.83/-0.83
3SIA+3He	12.75	2.54/-0.94

reflected in the E_i, as seen in Table 3. These values are consistent with those obtained in the previous two subsections, where removing a He involves positive interaction energies between 1.53 and 2.96 eV, while removing a SIA results in negative energies, or a single very low positive value for the SIA+2 He case. In addition, there seems to be a trend in the interaction energy when removing a He atom, whereby for a given number of SIAs, the interaction energy value decreases as the number of He atoms increases. Moreover, in the cases where the He atoms recombine with the vacancy, there appears to be little difference in the corresponding energy values, with the possible exception of the SIA+3 He case. However, for the cases involving 3 SIAs, the interaction energy values increase significantly, by about 1 eV, as compared to the other cases, as can be seen in the values corresponding to He in the third column of Table 3. This seems reasonable since, again, it is one of the 3 SIAs that recombines with the vacancy and not any of the He atoms, so the He is forced to sit at the charge density minima of the interface, which are less hollow (see Fig. 1 d) and e)). On the other hand, the negative interaction energy values as a result of a SIA removal (again with the exception of the very low positive 0.06 eV in the SIA+2 He case) suggest that the insertion of SIAs rather than He interstitials at the GB is energetically favored.

To complement the previous assessment, Table 4 shows the charge and atomic volume results of a Bader analysis performed for all calculated configurations by following the procedure reported in Ref. [76]. It seems that, depending on the specific case, a smaller atomic volume may correspond to a higher charge value for a given configuration, which makes sense since a larger available volume implies weaker atomic bonds and consequently fewer shared electrons with the corresponding implication on the charge density. If we compare the SIA volumes with the average volume of the W atoms on the top surface, which is about 16.85 $Å^3$ (charge ≈ 6 e, that is, the 6 valence band electrons of pure W), we can observe that the interstitial free volumes are slightly

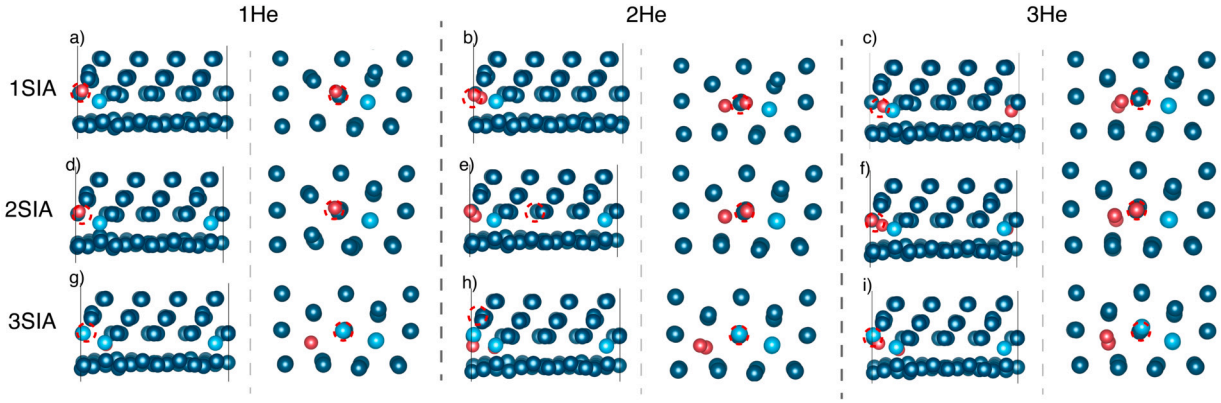

Fig. 6. (color on-line) YZ-plane (left column) and XZ-plane (right column) view of the 9 different relaxed SIA-He configurations. The three upper layers belong to the W⟨112⟩ surface, while the lower one belongs to the W⟨110⟩ surface. Light blue and red spheres correspond, respectively, to SIA and He. The red dashed circle indicates the position of the vacancy.

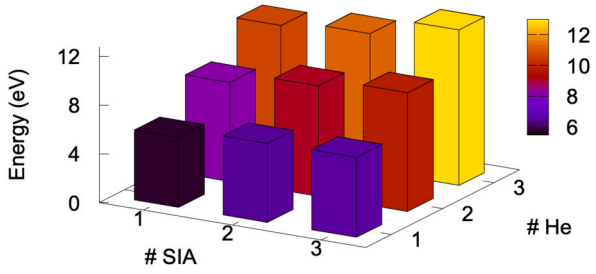

Fig. 7. Formation energies in eV as a function of the number of SIA and He.

smaller, except in the cases of single SIAs and an odd number of He atoms, where they are close nonetheless. This difference becomes even more pronounced if we consider the volume of the W atoms in the first layer (closest to the GB) of the top surface, with an atomic volume of about 17.5 Å^3. Therefore, it seems reasonable that the charge values are higher than 6 *e*. However, there are three cases where these values are basically 6 *e*, corresponding to the configurations with 3 SIAs and, in particular, for the SIA that recombines with the vacancy. This could somehow confirm that the SIA-vacancy recombination restores the electronic environment of a lattice atom. However, there is no clear general trend in the charges. The charge of the SIA does not seem to be affected by the presence of 1 or more He atoms. Regarding He, we see that for the cases with 1-2 SIA, i.e., the cases where He preferentially occupies the vacancy after relaxation, the atomic volumes are very similar. However, when SIA-vacancy recombination occurs, the volume of He is slightly smaller than in the previous arrangements. Comparing the charge density plots, it makes sense that the atomic volumes of the He atoms are larger when they are in the vacancy, as seen in Fig. 1 d) and e), since both the regions of lower charge density and the physical space available are larger.

Since SIAs recombine with the vacancy only when 3 SIAs are present, the next step is to estimate the energy cost for a single SIA to recombine with the vacancy. For this purpose, we have performed migration calculations using the NEB method [65] to find the energetic barrier of the motion of a SIA from the interstitial to the vacancy position in the presence of He atoms. Results are illustrated in Fig. 8. To prevent He atoms from recombining with the vacancy during the relaxation of the initial state, their positions were kept fixed. It is important to note that while SIA-V recombination is the most energetically favorable configuration, it is kinetically inaccessible at low temperatures due to the high migration barrier and the rapidity with which He atoms tend to occupy the vacancy, leading to a metastable configuration. Results in Fig. 8 show in the first place that, when only a single He atom is present, the final arrangement with the recombined SIA-V and the He fixed in the groove is 3.87 eV more stable than the configuration where both SIA and He remain in their interstitial positions. The energy barrier was found to be 0.54 eV, which is about 1 eV more favorable than the corresponding SIA migration along the direction parallel to the grooves formed by the W⟨112⟩ surface, namely, 1.6 eV, as obtained in Ref. [37]. When a first and a second additional He atom are introduced sequentially, the barrier takes values of 0.66 eV and 0.69 eV, respectively, i.e. the pres-

Table 4
Charge and atomic volume (At Vol) results of a Bader analysis in the presence of SIA and He at the GB. The ordering of the values is consistent with the notation used for each aggregate, i.e., the SIAs appear first and then the He.

Cluster (+vac)	Charge (*e*)	At Vol (Å^3)
SIA+He	6.15	16.96
	2.11	4.77
SIA+2He	6.11	16.58
	2.10	4.54
	2.12	5.01
SIA+3He	6.14	16.86
	2.09	4.40
	2.11	5.19
	2.09	4.27
2SIA+He	6.20	15.98
	6.05	16.02
	2.12	4.88
2SIA+2He	6.17	15.88
	5.99	15.52
	2.10	4.58
	2.11	4.93
2SIA+3He	6.17	15.89
	6.01	15.77
	2.08	4.38
	2.11	5.04
	2.08	4.44
3SIA+He	6.18	15.29
	6.01	16.59
	6.10	15.02
	2.12	3.97
3SIA+2He	6.16	15.24
	5.99	16.65
	6.12	15.07
	2.11	3.94
	2.13	3.98
3SIA+3He	6.15	15.25
	5.98	16.54
	6.14	15.11
	2.11	3.92
	2.09	3.81
	2.11	4.04

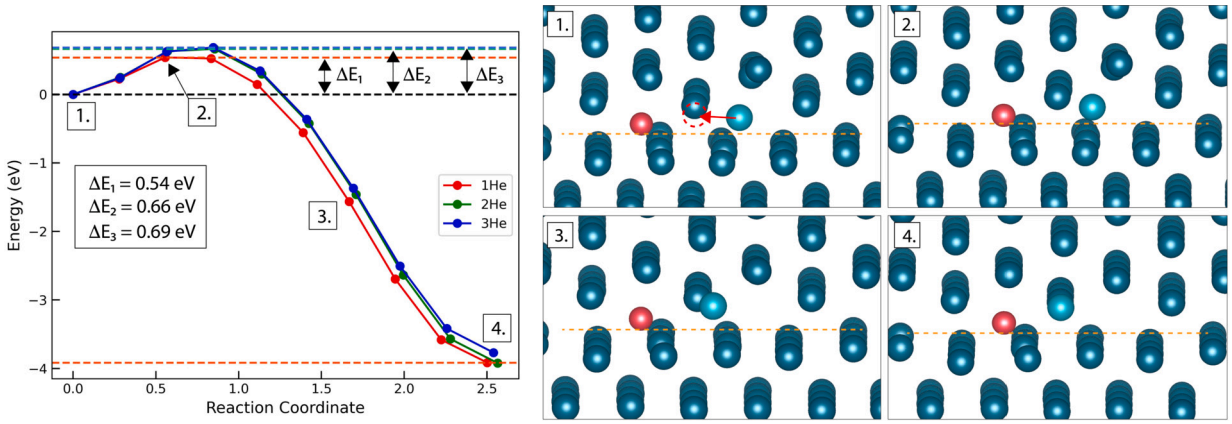

Fig. 8. (Left) Migration barrier of a SIA forced to recombine with the most stable vacancy in the presence of fixed He atoms. (Right) Sketch of the migration process of a SIA (light blue) with a single He atom (solid red) present. The dashed red circle corresponds to the vacancy position.

ence of additional He atoms, as described later, changes the migration energy of the SIA (see Fig. 8). This clearly indicates that, as the number of pre-existing He atoms at the interface increases, the eventual SIA-vacancy recombination becomes more difficult. However, this point still needs to be clarified, since it might be the case that, with more than 3 He atoms, the barrier height tends to reach an approximately constant value. Moreover, if the energy of the "forced" SIA-V recombination case is compared with the configuration where the He atoms are not fixed, the latter is still less favorable energetically by 2.33 eV. Therefore, at temperatures high enough to overcome the mentioned barrier, the system might eventually tend to recover its original structure in order to minimize its energy. The migration process of a SIA in the presence of a He atom is shown in the four snapshots on the right side of Fig. 8, where each image corresponds to a specific energy barrier indicated in the accompanying plot on the left side. For clarity, the path that the atom will follow is signaled by a red arrow and the position of the vacancy is indicated by a dashed red circle, respectively. The first figure shows the initial state, with the SIA in its interstitial position, and the second one illustrates a snapshot at the maximum of the migration barrier, as can be seen in the plot on the left.

Furthermore, for the configuration with 3 SIAs, we have calculated the migration of a He atom along the groove for the cases with 1, 2, and 3 He atoms to examine if, once the SIA is recombined with the vacancy, they prefer to aggregate near the other SIAs or, at a certain temperature, they tend to disperse along the groove in this type of interface. For the case of a single He atom, the migration barrier is 0.34 eV, the final state being 0.08 eV more stable than the state where the He atom is nearer to the other defects. This could be due to the fact that the closer presence of SIAs in the initial configuration modifies the charge density environment, pushing the He to minima in the GB with lower charge density. If we have 2 He atoms and move one of them along the groove, this migration barrier increases to 0.46 eV, i.e., 0.12 eV larger than for the single He atom case, but still 1.14 eV smaller than the migration of a single SIA along the groove. However, it is interesting to note that in this case the final state is 0.02 eV less stable, somehow evidencing the willingness of the He atoms to join together. This can be understood as being caused by mechanical effects. The first He produces a deformation on its surrounding atomic environment at the expense of an energetic cost. If the second He atom is placed far away, a similar energy cost can be expected, while for a position close to the first atom this value is reduced. Finally, if the migration process of one of the 3 He atoms is simulated, the migration barrier obtained remains at 0.46 eV. Moreover, the energy of the final state increases to a value 0.17 eV higher than that of the initial state, revealing, as expected, the great tendency for He atoms to cluster as their initial number increases.

Hence, looking at the results obtained from the migrations, both the barriers and the initial and final state energies, as well as at the formation and interaction energy values, it seems that, at low temperatures and when the density of SIA in the GB is not very high, the SIA will tend to align in rows along the GB instead of migrating to nearby vacancies. This behavior is well illustrated in Fig. 9, where we represent the unrelaxed (left) and relaxed (right) state for 2SIA+2He and for 3SIA+2He from two different perspectives. Again, the vacancy is indicated by a dashed red circle.

When the system with 2 SIAs and 2 He atoms is relaxed, as shown on the top right, the He atoms occupy the vacancy position, since, as mentioned before, the charge density in this region is lower. It is worth noting that, from the perspective of the XZ plane, the positions of the SIAs appear to be at the center of the pentagon formed by the lattice W atoms located in the nearby row, 3 rows belonging to the top surface and 2 rows to the bottom surface. From the perspective of the YZ plane, they appear to be aligned in a straight line with respect to the W atoms on the previous surface, as indicated by the yellow line, thereby seemingly attempting to create a new layer with the same structure as the upper W⟨112⟩ interface layer. In fact, referring back to Fig. 1 d) and e), these positions also seem to correspond to the regions of minimum charge density through the Y-axis. It seems that the top surface has a greater influence on the behavior of defects in the GB. Now, if we look at the lower part of Fig. 1, where 3 SIAs and 2 He atoms are present, the opposite behavior is observed since the SIA in the GB tend to occupy the specific positions mentioned above. Then, in this configuration there are 3 SIAs in between two successive stable positions, one of the SIA defects (the middle one) prefers to migrate to the vacancy position, with a migration barrier of about 0.6 eV (as seen in Fig. 8) depending on the number of He atoms, approximately 1 eV less than the migration barrier of a SIA to occupy the next stable position in the GB. On the other hand, the He atoms seem to occupy slightly different positions compared to the regions of minimum charge density shown in Fig. 1 d) and e), suggesting that the SIA slightly affects the charge density of the adjacent grooves.

3.4. SIA, He and H aggregates in the presence of the most stable vacancy

Finally, we analyze the coexistence of the 3 types of defects, in addition to the always present most stable vacancy. Although we expect a He to occupy the vacancy when we have 1-2 SIAs, and a SIA when we have 3 of them, we would like to assess, mainly from the energetic point of view, if H plays a transcendental role or not in this recombination process. In other words, our goal is to check if H influences (promoting or hindering) the recombination of the other defects with the vacancy, as well as discerning whether the other two types of defects contribute to stabilise the H in their vicinity or not. To do that, we start by describing the environment of the H atoms. First, we calculate the distance between H atoms and the minimum distance between

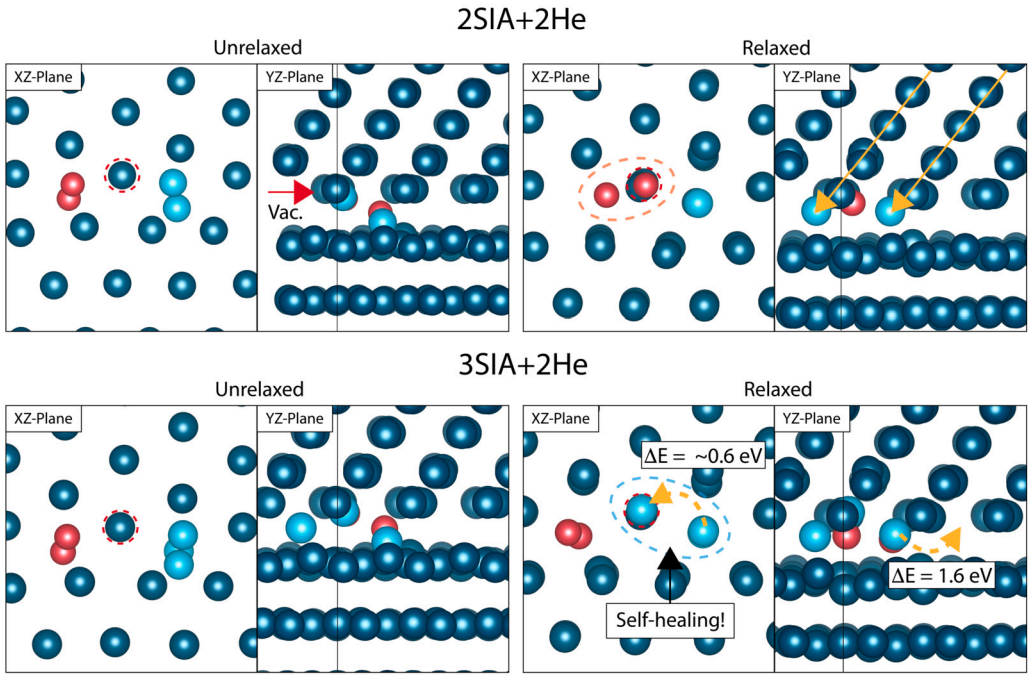

Fig. 9. (Top) Zoom image of the 2 SIA+2 He configuration before (left) and after (right) relaxation, viewed from the XZ and the YZ planes, respectively. Light blue and red spheres correspond, respectively, to SIA and He. (Bottom) *Idem* for the 3SIA+2He case. The outlined energy values give the migration barriers corresponding to the process sketched by the yellow dashed lines. The red dashed circles indicate the position of the vacancy.

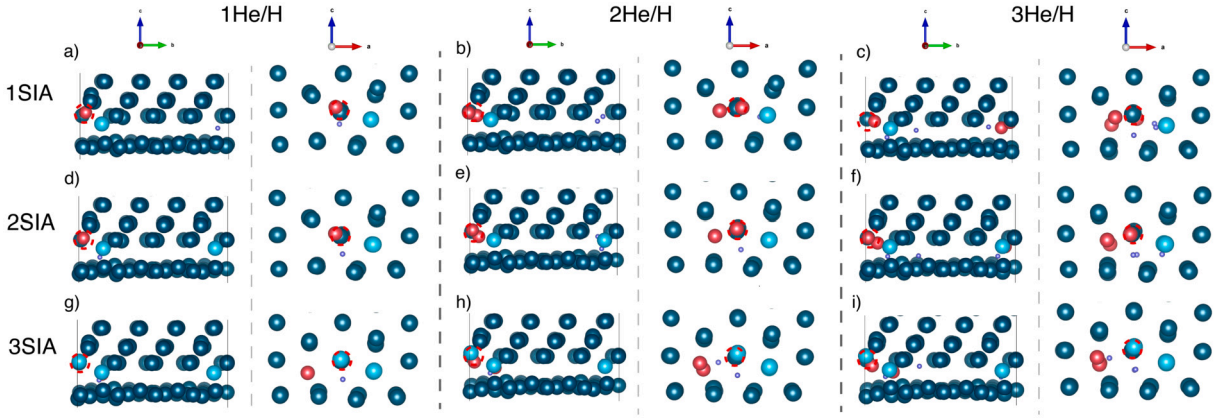

Fig. 10. (color on-line) YZ-plane (left column) and XZ-plane (right column) view of the 9 different relaxed SIA-He-H configurations. The three upper layers belong to the W⟨112⟩ surface, while the lower one belongs to the W⟨110⟩ surface. Light blue, red and purple spheres correspond, respectively, to SIA, He and H. The red dashed circles indicate the position of the vacancy.

a H and the nearest W atom, again to find out if they form H_2 or if they form WH, respectively. The calculated distances between H atoms ranges from 1.90 to 3.12 Å for the configurations with 2 He atoms and 2 H atoms, corresponding the minimum distance to the 2 SIA+2 He+2 H configuration and from 2.61 to 3.72 Å for the cases with 3He and 3H. Although the minimum distance between the H atoms is slightly smaller than those observed in the previous sections, it is still much larger than the distance at which the H_2 molecule could be considered to be formed (the aforementioned 0.74 Å). If we now look at the minimum distances between H and the W nearest atom, their values range from 1.69 to 1.99 Å, numbers slightly below the distance between H atoms themselves.

On the other hand, as expected, Voronoi volumes for the SIAs decrease as they have LIAs around them. These values range from 15.1 $Å^3$, for the SIA+He+H configuration, to 12.28 $Å^3$, for the 3 SIA+3 He+3 H configuration. However, this fact does not seem to play a relevant role neither in the recombination process, nor in how comfortable the SIAs are in the positions inside the GB.

This can be assessed by means of the formation energies, E_f, which are quite similar to those for the SIA+He case, i.e., the number of SIAs and He (H) atoms increases E_f, especially for the latter (see Fig. 11). The third column of Table 5 shows E_f differences between SIA-He-H and SIA-He cases. As it can be seen, there does not seem to be a clear trend. However, care must be taken when comparing these values, since the initial positions of the defects were not identical. Finally, we find that the interaction energies, E_i, are similar to the previous cases, namely, with values close to 0 for H (from -0.37 to 0.16 eV), positive for He (from 1.50 to 2.85 eV) and negative in most cases for SIA (from -1.81 to -0.16 eV), with only two small positive values when just a SIA and more than one LIA of each type is present. This is again consistent with our previous discussions. These near-zero, often negative, values of E_i for H suggest that H atoms are comfortable around He atoms [71,77], where they seemingly get pinned, so that their mobility is reduced.

Table 5
Formation (E_f) and interaction (E_i) energies in eV for different SIA-He-H combinations at the GB.

Cluster (+vac)	E_f (eV)	E_f(SIA-He-H) - E_f(SIA-He) (eV)	E_i H/He/SIA (eV)
SIA+He+H	5.59	-0.13	-0.22/1.80/-0.16
SIA+2He+2H	7.56	-0.56	-0.37/1.74/0.05
SIA+3He+3H	10.48	-0.18	-0.01/1.81/0.38
2SIA+He+H	6.55	0.07	-0.03/1.62/-1.09
2SIA+2He+2H	8.90	-0.16	0.06/1.83/-0.76
2SIA+3He+3H	11.43	1.70	0.08/1.50/-0.98
3SIA+He+H	6.82	0.26	0.16/2.85/-1.81
3SIA+2He+2He	9.87	-1.35	0.08/2.49/-0.69
3SIA+3He+3H	13.15	0.40	-0.03/2.44/-0.60

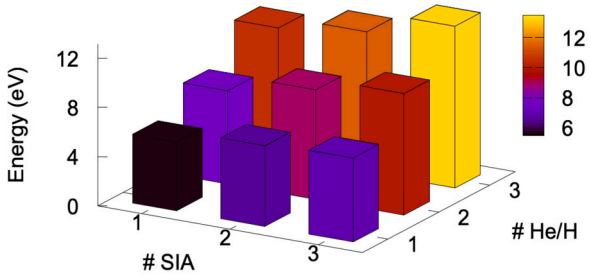

Fig. 11. Formation energies in eV as a function of the number of SIA and He/H.

4. Discussion

The above results reveal significant insights into the behavior of SIAs, He, and H within the GB in the presence of the most stable vacancy.

The presence of H does not significantly influence the behavior of the SIAs concerning their migration energies and chances of recombination with the vacancy. However, the presence of He notably influences the behavior of the SIAs and is dependent on the number of He atoms and SIAs. The first remarkable result is that He compete with the SIA to occupy the vacancy located at the GB. From the presented data, we deduce that the SIA occupy the vacancy, leading to self-healing behavior, if the number of SIAs is larger than that of He atoms. If this is not the case, the SIAs remain accommodated along a groove at the interface rather than filling the vacancy. This is so, because there is enough space available at the interface, so that it is energetically costlier for them to migrate to the vacancy than to accommodate close to the neighboring W atoms. In principle, and according to SRIM calculations [78] in nuclear fusion reactors operated in the direct drive laser approach, the number of available interstitials produced by He and H impinging into the reactor wall at an average energy of 3.81 MeV and 2.55 MeV [54], respectively, will be two and four orders of magnitude lower than the number of implanted He and H atoms. Thus, in a real scenario the number of SIAs is expected to be orders of magnitude lower than the number of LIAs, meaning that the self-healing process could be hindered by the presence of LIAs, a strongly relevant concern in developing alternative PFMs for these reactors. It is also important to mention that, considering the formation energies shown in Table 5, it is observed that H atoms are pinned in regions close to He atoms, where they feel more comfortable. This could negatively influence (delay/hamper) the H out-diffusion process via GBs previously observed in NW samples with a large GB density implanted only with H [79–82]. In light of this, gaining a deeper understanding of how He affects H out-diffusion, which in turn significantly influences material swelling, remains an important area for future investigation.

Nevertheless, we should bear in mind that all the results presented here are calculated at a temperature of 0 K. However, from the activation energies and migration barriers shown in subsection 3.3, one can speculate what would happen at higher temperatures (e.g., those expected in nuclear fusion reactors). To do this, we have to consider that the activation energies required to overcome the migration barriers calculated by means of NEB techniques should be seen as statistically significant values that provide a qualitative picture, implying that a lower barrier requires lower temperatures to be overcome, and thus the corresponding migration event is more likely on average, and the defects would choose this pathway. Therefore, if vacancies are available near the interface, it is likely that the SIAs will occupy them in order to minimize the energy of the system, especially at high SIA densities, as we observed in the energetic analysis. This phenomenon, where SIAs in the GB recombine with surrounding vacancies, is known as dynamic reflection or emission of interstitials [83]. However, for this to happen, it is crucial to determine which type of defect will populate the GBs first, since both SIAs and He tend to migrate towards them at very low temperatures [84]. If it is the He that fills them first, bubbles would form at the GB before the SIAs are able to recombine with the vacancies and the material could fail due to grain decohesion [85]. Further analysis of this issue is critical to understand, in this particular type of interface, to what extent the GB would delay bubble over-pressurization and whether, under certain conditions, He clusters could expand along the grooves without leading to grain decohesion and swelling.

Another interesting aspect is that the presented data show the absence of formation of H_2 or W hydrides. This could occur because the elastic binding effect is counterbalanced by the change in the effective position of the H states within the electronic structure. When the H ions are positioned close together, the bonding and anti-bonding states experience an upward asymmetric energy shift, leading to an increase in the interaction energy, resulting in a weak repulsion rather than the weak attraction predicted by a purely elastic analysis. This asymmetric splitting depends on the distances between the hydrogens in the same way as the elastic interaction.

Further analysis of this issue is crucial to understand, in this particular type of interface, to what extent the GB would delay bubble over-pressurization and whether, under certain conditions, He clusters could expand along the grooves without leading to grain decohesion and swelling.

5. Conclusions and outlook

In this study, we have used DFT calculations to investigate the possible influence of light impurity atoms (helium and hydrogen) on the recombination of self-interstitial atoms with the most stable vacancy in a W⟨110⟩/W⟨112⟩ GB, introducing up to three defects of each type. The coexistence of the three point defects studied suggests that the eagerness of the SIA to occupy the closest vacancy might be frustrated by the simultaneous presence of He, whereas the presence of H does not seem to have any influence on the SIA-vacancy recombination. Our results indicate that, initially, when the number of SIAs in the GB is ≤ 2, they prefer to stay along a row at the interface, since the energy required for them to accommodate within the GB is lower (about 0.6 eV) than that needed to migrate to the interface, and consequently He atoms would be the first to occupy the vacancy. However, when the number of SIAs is higher than 2, it is easier for them to recombine with nearby vacancies than to move along the grooves, since the latter migration is about

1 eV higher. The presence of He also affects the migration energy of the SIAs, that is decreased. An open question is still to elucidate if the He atoms are already aggregated in the vacancies at the interface and begin to populate the GB forming nanobubbles, before a high density of SIAs is reached. The study of such a process would require multiscale methods (DFT, MD and KMC - Kinetic Monte Carlo) to be fully understood.

In that regard, and in our opinion, the calculations and specific methodologies presented in this paper could be used to parametrize those multiscale modeling computational codes in complex grain boundary geometries.

CRediT authorship contribution statement

J. Suárez-Recio: Writing – review & editing, Writing – original draft, Visualization, Validation, Methodology, Investigation, Formal analysis, Conceptualization. **D. Fernández-Pello:** Methodology, Formal analysis. **M.A. Cerdeira:** Formal analysis. **C. González:** Validation, Methodology, Formal analysis. **R. Gonzalez-Arrabal:** Writing – review & editing, Supervision, Resources, Project administration, Methodology, Investigation, Funding acquisition, Formal analysis. **R. Iglesias:** Writing – review & editing, Validation, Supervision, Methodology, Investigation, Formal analysis, Conceptualization.

Declaration of competing interest

The authors declare the following financial interests/personal relationships which may be considered as potential competing interests: Jorge Suarez-Recio reports financial support was provided by Spain Ministry of Science and Innovation. Raquel Gonzalez-Arrabal reports financial support was provided by European Consortium for the Development of Fusion Energy. Roberto Iglesias reports financial support was provided by EIT RawMaterials GmbH (UE-22-EXPSKILLS-21104). Roberto Iglesias reports equipment, drugs, or supplies was provided by Supercomputational Network RES. Roberto Iglesias reports financial support was provided by Foundation for the Promotion in Asturias of Applied Scientific Research and Technology (SV-PA-21-AYUD/2021/51822). Cesar Gonzalez reports financial support was provided by Spain Ministry of Science and Innovation (PRE2020-096178). Jorge Suarez-Recio reports equipment, drugs, or supplies was provided by Polytechnic University of Madrid Supercomputing and Visualization Center of Madrid. If there are other authors, they declare that they have no known competing financial interests or personal relationships that could have appeared to influence the work reported in this paper.

Acknowledgements

This research was funded by the Spanish Ministry of Science and Innovation, through the predoctoral contract PRE2020-096178, by the project RADIAFUS V, grant PID2019-105325RB-C32, by the Convenio Plurianual con la Universidad Politécnica de Madrid en la línea de actuación “Programa de Excelencia para el Profesorado Universitario of the CAM” (PID2019-105325RB-C32). It has also has been partially funded under Eurofusion Enable Research grant CfP-FSD-AWP21-ENR-01 (2021–2025). RI acknowledges funding from the EIT-RM/EU, project ExpSkills-REM, grant number UE-22-EXPSKILLS-21104, and FICYT project MAGNES, grant SV-PA-21-AYUD/2021/51822. CG acknowledges financial support from the Spanish Ministry of Science, Innovation and Universities via the project PID2021-123112OB-C21. CG, JSR and RI are thankful to the Spanish Supercomputational Network RES for the computational resources provided by the Altamira (IFCA) supercomputer via projects FI-2023-1-0016 (CG) and QHS-2021-3-0005 (JSR-RI), respectively. The authors would like to express their gratitude to the support team at the Centre for Supercomputation and Visualisation in Madrid (CeSViMa).

Data availability

Data will be made available on request.

References

[1] H. Abu-Shawareb, et al., Lawson criterion for ignition exceeded in an inertial fusion experiment, Phys. Rev. Lett. 129 (2022) 075001, https://doi.org/10.1103/PhysRevLett.129.075001, https://link.aps.org/doi/10.1103/PhysRevLett.129.075001.

[2] A.L. Kritcher, et al., Design of an inertial fusion experiment exceeding the Lawson criterion for ignition, Phys. Rev. E 106 (2022) 025201, https://doi.org/10.1103/PhysRevE.106.025201, https://link.aps.org/doi/10.1103/PhysRevE.106.025201.

[3] A.B. Zylstra, et al., Experimental achievement and signatures of ignition at the national ignition facility, Phys. Rev. E 106 (2022) 025202, https://doi.org/10.1103/PhysRevE.106.025202, https://link.aps.org/doi/10.1103/PhysRevE.106.025202.

[4] D. Maisonnier, D. Campbell, I. Cook, L.D. Pace, L. Giancarli, J. Hayward, A.L. Puma, M. Medrano, P. Norajitra, M. Roccella, P. Sardain, M. Tran, D. Ward, Power plant conceptual studies in Europe, Nucl. Fusion 47 (11) (2007) 1524, https://doi.org/10.1088/0029-5515/47/11/014, https://dx.doi.org/10.1088/0029-5515/47/11/014.

[5] A. Wronski, A. Foukdeux, The ductile-brittle transition in polycrystalline tungsten, J. Less-Common Met. 8 (3) (1965) 149–158, https://doi.org/10.1016/0022-5088(65)90042-1, https://www.sciencedirect.com/science/article/pii/0022508865900421.

[6] D. Cereceda, M. Diehl, F. Roters, D. Raabe, J.M. Perlado, J. Marian, Unraveling the temperature dependence of the yield strength in single-crystal tungsten using atomistically-informed crystal plasticity calculations, Int. J. Plast. 78 (2016) 242–265, https://doi.org/10.1016/j.ijplas.2015.09.002, https://www.sciencedirect.com/science/article/pii/S0749641915001485.

[7] T. Loewenhoff, J. Linke, G. Pintsuk, C. Thomser, Tungsten and cfc degradation under combined high cycle transient and steady state heat loads, Fusion Eng. Des. 87 (7) (2012) 1201–1205, https://doi.org/10.1016/j.fusengdes.2012.02.106, tenth International Symposium on Fusion Nuclear Technology (ISFNT-10), https://www.sciencedirect.com/science/article/pii/S0920379612001809.

[8] J. Boisse, C. Domain, C. Becquart, Modelling self trapping and trap mutation in tungsten using dft and molecular dynamics with an empirical potential based on dft, J. Nucl. Mater. 455 (1) (2014) 10–15, https://doi.org/10.1016/j.jnucmat.2014.02.031, proceedings of the 16th International Conference on Fusion Reactor Materials (ICFRM-16), https://www.sciencedirect.com/science/article/pii/S0022311514001032.

[9] S.J. Zenobia, R. Radel, B. Cipiti, G.L. Kulcinski, High temperature surface effects of He+ implantation in icf fusion first wall materials, J. Nucl. Mater. 389 (2) (2009) 213–220, https://doi.org/10.1016/j.jnucmat.2009.02.004, particle Beam Induced Radiation Effects in Materials, https://www.sciencedirect.com/science/article/pii/S0022311509003420.

[10] R.A. Causey, T.J. Venhaus, The use of tungsten in fusion reactors: a review of the hydrogen retention and migration properties, Phys. Scr. 2001 (T94) (2001) 9, https://doi.org/10.1238/Physica.Topical.094a00009.

[11] G. Pintsuk, Tungsten as a plasma-facing material, Compr. Nucl. Mater. 4 (2012) 551–581, https://doi.org/10.1016/B978-0-08-056033-5.00118-X.

[12] N. Dutta, N. Buzarbaruah, S. Mohanty, Damage studies on tungsten due to helium ion irradiation, J. Nucl. Mater. 452 (1) (2014) 51–56, https://doi.org/10.1016/j.jnucmat.2014.04.032, https://www.sciencedirect.com/science/article/pii/S0022311514002475.

[13] O. El-Atwani, K. Hattar, J. Hinks, G. Greaves, S. Harilal, A. Hassanein, Helium bubble formation in ultrafine and nanocrystalline tungsten under different extreme conditions, J. Nucl. Mater. 458 (2015) 216–223, https://doi.org/10.1016/j.jnucmat.2014.12.095, https://www.sciencedirect.com/science/article/pii/S0022311514010472.

[14] N. Enomoto, S. Muto, T. Tanabe, J. Davis, A. Haasz, Grazing-incidence electron microscopy of surface blisters in single- and polycrystalline tungsten formed by H+, D+ and He+ irradiation, J. Nucl. Mater. 385 (3) (2009) 606–614, https://doi.org/10.1016/j.jnucmat.2009.01.298, https://www.sciencedirect.com/science/article/pii/S0022311509003213.

[15] S. Gilliam, S. Gidcumb, N. Parikh, D. Forsythe, B. Patnaik, J. Hunn, L. Snead, G. Lamaze, Retention and surface blistering of helium irradiated tungsten as a first wall material, J. Nucl. Mater. 347 (3) (2005) 289–297, https://doi.org/10.1016/j.jnucmat.2005.08.017, laser Fusion Materials, https://www.sciencedirect.com/science/article/pii/S0022311505004101.

[16] D. Nishijima, M. Ye, N. Ohno, S. Takamura, Formation mechanism of bubbles and holes on tungsten surface with low-energy and high-flux helium plasma irradiation in NAGDIS-II, J. Nucl. Mater. 329–333 (2004) 1029–1033, https://doi.org/10.1016/j.jnucmat.2004.04.129, proceedings of the 11th International Conference on Fusion Reactor Materials (ICFRM-11), https://www.sciencedirect.com/science/article/pii/S0022311504002934.

[17] T. Renk, P. Provencio, T. Tanaka, C. Olson, R. Peterson, J. Stolp, D. Schroen, T. Knowles, Chamber wall materials response to pulsed ions at power-plant level fluences, J. Nucl. Mater. 347 (3) (2005) 266–288, https://doi.org/10.1016/j.jnucmat.2005.08.021, laser Fusion Materials, https://www.sciencedirect.com/science/article/pii/S0022311505004095.

[18] A. Rivera, G. Valles, M. Caturla, I. Martin-Bragado, Effect of ion flux on helium retention in helium-irradiated tungsten, Nucl. Instrum. Methods Phys. Res., Sect. B, Beam Interact. Mater. Atoms 303 (2013), in: Proceedings of the 11th Computer Simulation of Radiation Effects in Solids (COSIRES) Conference Santa Fe, New Mexico, USA, July 24-29, 2012, pp. 81–83, https://www.sciencedirect.com/science/article/pii/S0168583X12006751.
[19] L. Gao, A. Manhard, W. Jacob, U. von Toussaint, M. Balden, K. Schmid, High-flux hydrogen irradiation-induced cracking of tungsten reproduced by low-flux plasma exposure, Nucl. Fusion 59 (5) (2019) 056023, https://doi.org/10.1088/1741-4326/ab0915, https://dx.doi.org/10.1088/1741-4326/ab0915.
[20] A. Haasz, J. Davis, M. Poon, R. Macaulay-Newcombe, Deuterium retention in tungsten for fusion use, J. Nucl. Mater. 258 (263) (1998) 889–895, https://doi.org/10.1016/S0022-3115(98)00072-5, https://www.sciencedirect.com/science/article/pii/S0022311598000725.
[21] F. Liu, Y. Zhang, W. Han, J. Yu, G. Lu, K. Zhu, Investigation of hydrogen behavior in tungsten exposed to high energy hydrogen plasma, Nucl. Instrum. Methods Phys. Res., Sect. B, Beam Interact. Mater. Atoms 307 (2013) 320–323, https://doi.org/10.1016/j.nimb.2012.11.069, the 18th International Conference on Ion Beam Modifications of Materials (IBMM2012), https://www.sciencedirect.com/science/article/pii/S0168583X13000773.
[22] J. Roth, K. Schmid, Hydrogen in tungsten as plasma-facing material, Phys. Scr. 2011 (T145) (2011) 014031, https://doi.org/10.1088/0031-8949/2011/T145/014031, https://dx.doi.org/10.1088/0031-8949/2011/T145/014031.
[23] Y. Ueda, T. Funabiki, T. Shimada, K. Fukumoto, H. Kurishita, M. Nishikawa, Hydrogen blister formation and cracking behavior for various tungsten materials, J. Nucl. Mater. 337–339 (2005) 1010–1014, https://doi.org/10.1016/j.jnucmat.2004.10.077, pSI-16, https://www.sciencedirect.com/science/article/pii/S0022311504008475.
[24] M. Ye, H. Kanehara, S. Fukuta, N. Ohno, S. Takamura, Blister formation on tungsten surface under low energy and high flux hydrogen plasma irradiation in NAGDIS-I, J. Nucl. Mater. 313–316 (2003) 72–76, https://doi.org/10.1016/S0022-3115(02)01349-1, plasma-Surface Interactions in Controlled Fusion Devices 15, https://www.sciencedirect.com/science/article/pii/S0022311502013491.
[25] R. Abernethy, Predicting the performance of tungsten in a fusion environment: a literature review, Mater. Sci. Technol. 33 (2016) 1–12, https://doi.org/10.1080/02670836.2016.1185260.
[26] M. Gilbert, J.-C. Sublet, Neutron-induced transmutation effects in w and w-alloys in a fusion environment, Nucl. Fusion 51 (4) (2011) 043005, https://doi.org/10.1088/0029-5515/51/4/043005.
[27] V. Alimov, Y. Hatano, K. Sugiyama, M. Balden, M. Oyaidzu, S. Akamaru, K. Tada, H. Kurishita, T. Hayashi, M. Matsuyama, Surface morphology and deuterium retention in tungsten and tungsten–rhenium alloy exposed to low-energy, high flux d plasma, J. Nucl. Mater. 454 (1) (2014) 136–141, https://doi.org/10.1016/j.jnucmat.2014.07.064, https://www.sciencedirect.com/science/article/pii/S0022311514005030.
[28] T. Renk, P. Provencio, a. Tanaka, J. Blanchard, b. Martin, T. Knowlesc, Survivability of first-wall materials in fusion devices: an experimental study of material exposure to pulsed energetic ions, Fusion Sci. Technol. 61 (2012) 57–80, https://doi.org/10.13182/FST12-A13339.
[29] A. Paramo, Effects of irradiation on plasma facing materials in hiper laser fusion power plant: silica final lenses and tungsten first wall, Ph. D. thesis, 07 2017.
[30] R. Gonzalez-Arrabal, A. Rivera, J.M. Perlado, Limitations for tungsten as plasma facing material in the diverse scenarios of the European inertial confinement fusion facility HiPER: current status and new approaches, Matter Radiat. Extrem. 5 (5) (2020) 055201, https://doi.org/10.1063/5.0010954, arXiv: https://pubs.aip.org/aip/mre/article-pdf/doi/10.1063/5.0010954/16056794/055201_1_online.pdf.
[31] O. El-Atwani, K. Hattar, J. Hinks, G. Greaves, S. Harilal, A. Hassanein, Helium bubble formation in ultrafine and nanocrystalline tungsten under different extreme conditions, J. Nucl. Mater. 458 (2015) 216–223, https://doi.org/10.1016/j.jnucmat.2014.12.095.
[32] R. Gonzalez-Arrabal, M. Panizo-Laiz, N. Gordillo, E. Tejado, F. Munnik, A. Rivera, J. Perlado, Hydrogen accumulation in nanostructured as compared to the coarse-grained tungsten, J. Nucl. Mater. 453 (1) (2014) 287–295, https://doi.org/10.1016/j.jnucmat.2014.06.057, https://www.sciencedirect.com/science/article/pii/S0022311514004140.
[33] C. González, M. Panizo-Laiz, N. Gordillo, C. Guerrero, E. Tejado, F. Munnik, P. Piaggi, E. Bringa, R. Iglesias, J. Perlado, R. González-Arrabal, H trapping and mobility in nanostructured tungsten grain boundaries: a combined experimental and theoretical approach, Nucl. Fusion 55 (11) (2015) 113009, https://doi.org/10.1088/0029-5515/55/11/113009.
[34] P. Piaggi, E. Bringa, R. Pasianot, N. Gordillo, M. Panizo-Laiz, J. del Río, C. Gómez de Castro, R. Gonzalez-Arrabal, Hydrogen diffusion and trapping in nanocrystalline tungsten, J. Nucl. Mater. 458 (2015) 233–239, https://doi.org/10.1016/j.jnucmat.2014.12.069, https://www.sciencedirect.com/science/article/pii/S0022311514010113.
[35] G. Valles, M. Panizo-Laiz, C. González, I. Martin-Bragado, R. González-Arrabal, N. Gordillo, R. Iglesias, C. Guerrero, J. Perlado, A. Rivera, Influence of grain boundaries on the radiation-induced defects and hydrogen in nanostructured and coarse-grained tungsten, Acta Mater. 122 (2017) 277–286, https://doi.org/10.1016/j.actamat.2016.10.007.
[36] M. Panizo-Laiz, P. Díaz-Rodríguez, A. Rivera, G. Valles, I. Martín-Bragado, J. Perlado, F. Munnik, R. González-Arrabal, Experimental and computational studies of the influence of grain boundaries and temperature on the radiation-induced damage and hydrogen behavior in tungsten, Nucl. Fusion 59 (8) (2019) 086055, https://doi.org/10.1088/1741-4326/ab26e9.
[37] D. Fernández-Pello, M. Cerdeira, J. Suárez-Recio, R. González-Arrabal, R. Iglesias, C. González, Coexistence of a self-interstitial atom with light impurities in a tungsten grain boundary, J. Nucl. Mater. 560 (2022) 153481, https://doi.org/10.1016/j.jnucmat.2021.153481, https://www.sciencedirect.com/science/article/pii/S0022311521007017.
[38] O. El-Atwani, J. Hinks, G. Greaves, S. Gonderman, T. Qiu, M. Efe, J. Allain, In-situ tem observation of the response of ultrafine- and nanocrystalline-grained tungsten to extreme irradiation environments, Sci. Rep. 4 (May 2014), https://doi.org/10.1038/srep04716.
[39] O. El-Atwani, C.N. Taylor, J. Frishkoff, W. Harlow, E. Esquivel, S.A. Maloy, M.L. Taheri, Thermal desorption spectroscopy of high fluence irradiated ultrafine and nanocrystalline tungsten: helium trapping and desorption correlated with morphology, Nucl. Fusion 58 (1) (2018) 016020, https://doi.org/10.1088/1741-4326/aa86cf.
[40] C. González, R. Iglesias, Cluster formation and eventual mobility of helium in a tungsten grain boundary, J. Nucl. Mater. 514 (2019) 171–180, https://doi.org/10.1016/j.jnucmat.2018.11.029.
[41] W.-J. Qin, W. Guo, T. Cheng, J. Tang, C.-Z. Jiang, F. Ren, Review on helium behaviors in nanochannel tungsten film, Tungsten 3 (07) (2021), https://doi.org/10.1007/s42864-021-00097-3.
[42] W. Qin, F. Ren, R.P. Doerner, G. Wei, Y. Lv, S. Chang, M. Tang, H. Deng, C. Jiang, Y. Wang, Nanochannel structures in w enhance radiation tolerance, Acta Mater. 153 (2018) 147–155, https://doi.org/10.1016/j.actamat.2018.04.048, https://www.sciencedirect.com/science/article/pii/S1359645418303252.
[43] W. Qin, F. Ren, J. Zhang, X. Dong, Y. Feng, H. Wang, J. Tang, G. Cai, Y. Wang, C. Jiang, Helium retention in krypton ion pre-irradiated nanochannel w film, Nucl. Fusion 58 (2) (2017) 026021, https://doi.org/10.1088/1741-4326/aa94f0.
[44] W. Qin, Y. Wang, M. Tang, F. Ren, Q. Fu, G. Cai, L. Dong, L. Hu, G. Wei, C. Jiang, Microstructure and hardness evolution of nanochannel w films irradiated by helium at high temperature, J. Nucl. Mater. 502 (2018) 132–140, https://doi.org/10.1016/j.jnucmat.2018.02.013, https://www.sciencedirect.com/science/article/pii/S0022311517313983.
[45] G. Wei, F. Ren, J. Fang, W. Hu, F. Gao, W. Qin, T. Cheng, Y. Wang, C. Jiang, H. Deng, Understanding the release of helium atoms from nanochannel tungsten: a molecular dynamics simulation, Nucl. Fusion 59 (7) (2019) 076020, https://doi.org/10.1088/1741-4326/ab14c7.
[46] A. Lopez-Cazalilla, C. Cupak, M. Fellinger, F. Granberg, P.S. Szabo, A. Mutzke, K. Nordlund, F. Aumayr, R. González-Arrabal, Comparative study regarding the sputtering yield of nanocolumnar tungsten surfaces under ar^+ irradiation, Phys. Rev. Mater. 6 (2022) 075402, https://doi.org/10.1103/PhysRevMaterials.6.075402.
[47] C. Cupak, A. Lopez-Cazalilla, H. Biber, J. Brötzner, M. Fellinger, F. Brandstätter, P.S. Szabo, A. Mutzke, F. Granberg, K. Nordlund, R. González-Arrabal, F. Aumayr, Sputter yield reduction and fluence stability of numerically optimized nanocolumnar tungsten surfaces, Phys. Rev. Mater. 7 (2023) 065406, https://doi.org/10.1103/PhysRevMaterials.7.065406.
[48] J. Brötzner, C. Cupak, M. Fellinger, H. Biber, A. Lopez-Cazalilla, F. Granberg, F. Kporha, A. Mutzke, R. González-Arrabal, F. Aumayr, Sputtering yield reduction for nano-columnar w surfaces under d ion irradiation, Nucl. Mater. Energy 37 (2023) 101507, https://doi.org/10.1016/j.nme.2023.101507, https://www.sciencedirect.com/science/article/pii/S2352179123001461.
[49] R. Gonzalez-Arrabal, Y. Mendez-González, J. Perlado, Sputtering fabrication of isolated w nanocolumns: a possible alternative as plasma facing material for nuclear fusion reactors, Nucl. Mater. Energy 40 (2024) 101704, https://doi.org/10.1016/j.nme.2024.101704, https://www.sciencedirect.com/science/article/pii/S2352179124001273.
[50] N. Gordillo, C. Gómez de Castro, E. Tejado, J. Pastor, G. Balabanian, M. Panizo-Laiz, R. Gonzalez-Arrabal, J. Perlado, J. del Rio, On the thermal stability of the nanostructured tungsten coatings, Surf. Coat. Technol. 325 (2017) 588–593, https://doi.org/10.1016/j.surfcoat.2017.06.070, https://www.sciencedirect.com/science/article/pii/S0257897217306849.
[51] M.J. Caturla, T. Diaz de la Rubia, M. Victoria, R. Corzine, M. James, G. Greene, Multiscale modeling of radiation damage: applications to damage production by GeV proton irradiation of Cu and W, and pulsed irradiation effects in Cu and Fe, J. Nucl. Mater. 296 (1) (2001) 90–100, https://doi.org/10.1016/S0022-3115(01)00569-4, 4th Int. Workshop on Spallation Materials Technology, https://www.sciencedirect.com/science/article/pii/S0022311501005694.
[52] I. Beyerlein, A. Caro, M. Demkowicz, N. Mara, A. Misra, B. Uberuaga, Radiation damage tolerant nanomaterials, Mater. Today 16 (11) (2013) 443–449, https://doi.org/10.1016/j.mattod.2013.10.019, https://www.sciencedirect.com/science/article/pii/S1369702113003581.
[53] X.-M. Bai, B.P. Uberuaga, The influence of grain boundaries on radiation-induced point defect production in materials: a review of atomistic studies, JOM - J. Miner. Met. Mater. Soc. 65 (3) (2013) 360–373, https://doi.org/10.1007/s11837-012-0544-5.
[54] D. Garoz, A. Páramo, A. Rivera, J. Perlado, R. González-Arrabal, Modelling the thermomechanical behaviour of the tungsten first wall in hiper laser fusion scenarios, Nucl. Fusion 56 (12) (2016) 126014, https://doi.org/10.1088/0029-5515/56/12/126014.

[55] H. Eleveld, A. van Veen, Void growth and thermal desorption of deuterium from voids in tungsten, J. Nucl. Mater. 212–215 (1994) 1421–1425, https://doi.org/10.1016/0022-3115(94)91062-6, https://www.sciencedirect.com/science/article/pii/0022311594910626.
[56] A. Debelle, M. Barthe, T. Sauvage, First temperature stage evolution of irradiation-induced defects in tungsten studied by positron annihilation spectroscopy, J. Nucl. Mater. 376 (2) (2008) 216–221, https://doi.org/10.1016/j.jnucmat.2008.03.002, https://www.sciencedirect.com/science/article/pii/S0022311508001724.
[57] P. Sahni, The Hohenberg-Kohn Theorems and Kohn-Sham Density Functional Theory, 2004, pp. 99–123.
[58] G. Kresse, J. Hafner, Ab initio molecular dynamics for liquid metals, Phys. Rev. B 47 (1993) 558–561, https://doi.org/10.1103/PhysRevB.47.558.
[59] P.E. Blöchl, Projector augmented-wave method, Phys. Rev. B 50 (1994) 17953–17979, https://doi.org/10.1103/PhysRevB.50.17953.
[60] J.P. Perdew, K. Burke, M. Ernzerhof, Generalized gradient approximation made simple, Phys. Rev. Lett. 77 (1996) 3865–3868, https://doi.org/10.1103/PhysRevLett.77.3865.
[61] A. James, M. Lord, Macmillan's Chemical and Physical Data, Macmillan, 1992, https://books.google.com/books?id=J386AQAAIAAJ.
[62] H. Grimmer, W. Bollmann, D.H. Warrington, Coincidence-site lattices and complete pattern-shift in cubic crystals, Acta Crystallogr., Sect. A 30 (2) (1974) 197–207, https://doi.org/10.1107/S056773947400043X.
[63] J.M. Kang, Voronoi Diagram, Springer US, Boston, MA, 2008, pp. 1232–1235.
[64] R.F. Bader, Atoms in Molecules: A Quantum Theory, Oxford University Press, 1990.
[65] D. Sheppard, R. Terrell, G. Henkelman, Optimization methods for finding minimum energy paths, J. Chem. Phys. 128 (13) (2008) 134106, https://doi.org/10.1063/1.2841941.
[66] K.J. Laidler, M.C. King, Development of transition-state theory, J. Phys. Chem. 87 (15) (1983) 2657–2664, https://doi.org/10.1021/j100238a002.
[67] E. Bitzek, P. Koskinen, F. Gähler, M. Moseler, P. Gumbsch, Structural relaxation made simple, Phys. Rev. Lett. 97 (2006) 170201, https://doi.org/10.1103/PhysRevLett.97.170201.
[68] L. Wei, J. Li, Y. Li, Q. Zheng, F. Cheng, C. Zhang, J. Li, G. Zhao, Z. Zeng, H dissolution and desorption near he-v complexes in w surfaces with different orientations, J. Nucl. Mater. 588 (2024) 154804, https://doi.org/10.1016/j.jnucmat.2023.154804, https://www.sciencedirect.com/science/article/pii/S0022311523005718.
[69] X. Jin, F. Djurabekova, E.A. Hodille, S. Markelj, K. Nordlund, Analysis of lattice locations of deuterium in tungsten and its application for predicting deuterium trapping conditions, Phys. Rev. Mater. 8 (2024) 043604, https://doi.org/10.1103/PhysRevMaterials.8.043604, https://link.aps.org/doi/10.1103/PhysRevMaterials.8.043604.
[70] C. Becquart, C. Domain, A density functional theory assessment of the clustering behaviour of He and H in tungsten, J. Nucl. Mater. 386–388 (2009) 109–111, https://doi.org/10.1016/j.jnucmat.2008.12.085, fusion Reactor Materials, https://www.sciencedirect.com/science/article/pii/S0022311508008179.
[71] H.-B. Zhou, Y.-L. Liu, S. Jin, Y. Zhang, G.-N. Luo, G.-H. Lu, Towards suppressing h blistering by investigating the physical origin of the h–he interaction in w, Nucl. Fusion 50 (11) (2010) 115010, https://doi.org/10.1088/0029-5515/50/11/115010.
[72] C. González, M. Cerdeira, S. Palacios, R. Iglesias, Reduction of the repulsive interaction as origin of helium trapping inside a monovacancy in bcc metals, J. Mater. Sci. 50 (05) (2015), https://doi.org/10.1007/s10853-015-8935-y.
[73] J.A. White, D.M. Bird, M.C. Payne, Dissociation of h_2 on w(100), Phys. Rev. B 53 (1996) 1667–1674, https://doi.org/10.1103/PhysRevB.53.1667, https://link.aps.org/doi/10.1103/PhysRevB.53.1667.
[74] W. Zheng, A. Gallagher, Hydrogen dissociation on high-temperature tungsten, Surf. Sci. 600 (10) (2006) 2207–2213, https://doi.org/10.1016/j.susc.2006.03.032, https://www.sciencedirect.com/science/article/pii/S0039602806002615.
[75] A. Rodríguez-Fernández, L. Bonnet, P. Larrégaray, R.D. Muiño, Ab initio molecular dynamics of hydrogen on tungsten surfaces, Phys. Chem. Chem. Phys. 23 (2021) 7919–7925, https://doi.org/10.1039/D0CP05423B.
[76] M. Yu, D.R. Trinkle, Accurate and efficient algorithm for Bader charge integration, J. Chem. Phys. 134 (6) (2011) 064111, https://doi.org/10.1063/1.3553716, arXiv: https://pubs.aip.org/aip/jcp/article-pdf/doi/10.1063/1.3553716/14735696/064111_1_online.pdf.
[77] C. Becquart, C. Domain, A density functional theory assessment of the clustering behaviour of He and H in tungsten, J. Nucl. Mater. 386–388 (2009) 109–111, https://doi.org/10.1016/j.jnucmat.2008.12.085.
[78] J. Ziegler, J. Manoyan, The stopping of ions in compounds, Nucl. Instrum. Methods Phys. Res., Sect. B, Beam Interact. Mater. Atoms 35 (3) (1988) 215–228, https://doi.org/10.1016/0168-583X(88)90273-X, https://www.sciencedirect.com/science/article/pii/0168583X8890273X.
[79] Z. Bergstrom, L. Yang, B. Wirth, An ab-initio study of hydrogen trapping energetics at bcc tungsten metal-noble gas interfaces, J. Nucl. Mater. 548 (2021) 152814, https://doi.org/10.1016/j.jnucmat.2021.152814, https://www.sciencedirect.com/science/article/pii/S0022311521000374.
[80] B. Jiang, F.R. Wan, W.T. Geng, Strong hydrogen trapping at helium in tungsten: density functional theory calculations, Phys. Rev. B 81 (2010) 134112, https://doi.org/10.1103/PhysRevB.81.134112, https://link.aps.org/doi/10.1103/PhysRevB.81.134112.
[81] S.-C. Lee, J.-H. Choi, J.G. Lee, Energetics of he and h atoms with vacancies in tungsten: first-principles approach, J. Nucl. Mater. 383 (3) (2009) 244–246, https://doi.org/10.1016/j.jnucmat.2008.09.017, https://www.sciencedirect.com/science/article/pii/S0022311508005370.
[82] X.-S. Kong, J. Hou, X.-Y. Li, X. Wu, C. Liu, J.-L. Chen, G.-N. Luo, First principles study of inert-gas (helium, neon, and argon) interactions with hydrogen in tungsten, J. Nucl. Mater. 487 (2017) 128–134, https://doi.org/10.1016/j.jnucmat.2017.01.038, https://www.sciencedirect.com/science/article/pii/S0022311516311801.
[83] X. Li, G. Duan, Y. Xu, Y. Zhang, W. Liu, C. Liu, Y. Liang, J.-L. Chen, G.-N. Luo, Annihilating vacancies via dynamic reflection and emission of interstitials in nanocrystal tungsten, Nucl. Fusion 57 (11) (2017) 116055, https://doi.org/10.1088/1741-4326/aa80a8.
[84] A.S. Soltan, R. Vassen, P. Jung, Migration and immobilization of hydrogen and helium in gold and tungsten at low temperatures, J. Appl. Phys. 70 (2) (1991) 793–797, https://doi.org/10.1063/1.349636, arXiv: https://pubs.aip.org/aip/jap/article-pdf/70/2/793/18644078/793_1_online.pdf.
[85] E. Martínez, B.P. Uberuaga, B.D. Wirth, Atomistic modeling of helium segregation to grain boundaries in tungsten and its effect on de-cohesion, Nucl. Fusion 57 (8) (2017) 086044, https://doi.org/10.1088/1741-4326/aa6e15.